

# PULSE-BY-PULSE BEAM PARAMETER SWITCHING OF HIGH-QUALITY BEAMS FOR MULTI-BEAMLINE OPERATION AT SACLA

H. Maesaka<sup>†</sup>, T. Fukui, T. Hara, RIKEN SPring-8 Center, 679-5148 Sayo, Hyogo, Japan  
N. Hosoda, C. Kondo<sup>1</sup>, S. Matsubara, T. Ohshima<sup>1</sup>, M. Yamaga, Y. Otake,  
Japan Synchrotron Radiation Research Institute 679-5198 Sayo, Hyogo, Japan  
T. Hasegawa, O. Morimoto, Y. Tajiri, S. Tanaka, M. Yoshioka,  
SPring-8 Service Co., Ltd. 679-5165 Tatsuno, Hyogo, Japan  
<sup>1</sup>also at RIKEN SPring-8 Center, 679-5148 Sayo, Hyogo, Japan

## Abstract

Since the number of beamlines in a linac-based X-ray free-electron laser (XFEL) facility is limited, it is quite important to increase the machine time for user experiments. In the XFEL facility, SACLA, a new XFEL beamline, BL2, was constructed in addition to the existing beamline, BL3, and a kicker magnet was installed into the beam switchyard to distribute a 60 Hz electron beam to both beamlines one after another. Since a beam energy and an optimum bunch length are usually different for each beamline, we developed a beam route and parameter switching software to change beam parameters pulse-by-pulse. The switching system successfully distributed high quality electron beams to both beamlines and XFEL performance for each beamline was individually optimized. When a high-quality electron beam having less than 1 mm mrad normalized emittance, 10 fs FWHM bunch length, 10 kA peak current, etc. was injected into BL2, however, the XFEL intensity of BL2 was significantly smaller than BL3 due to the growth of the emittance and pointing jitter coming from coherent synchrotron radiation (CSR). Therefore, we rearranged the optics of the transport line to mitigate the CSR effect and the XFEL intensity comparable to BL3 was achieved. We are also developing an on-demand beam route and parameter switching system needed for the beam injection from SACLA to the SPring-8 storage ring. The on-demand system also showed a sufficient performance and it will be used for the user operation in the near future.

## INTRODUCTION

Linac-based X-ray free-electron laser (XFEL) facilities were constructed for the past decade or so and they have contributed for various breakthroughs about microscopic phenomena. However, the number beamlines of an XFEL facility is much smaller than a ring-based light source. Therefore, increasing opportunities to use XFEL is quite important to maximize scientific outcomes.

The XFEL facility, SACLA, has been providing brilliant X-ray laser pulses since 2011 in a photon energy region from 4 keV to 20 keV [1]. SACLA mainly consists of a low-emittance thermionic electron gun [2] followed by sub-harmonic accelerators [3], C-band main accelerators up to 8 GeV [4] and XFEL beamlines with in-vacuum undulators, as shown in Fig. 1. The user operation of

SACLA started with one XFEL beamline, BL3, with a maximum repetition rate of 60 Hz. An additional XFEL beamline, BL2, was constructed in 2014 to double the user time effectively and a kicker magnet was also installed into the switchyard to switch the beam route pulse-by-pulse [5]. In addition, the SCSS test accelerator [6] was moved to SACLA-BL1 in 2014, the maximum beam energy was upgraded to 0.8 GeV in 2016, and it has been providing soft-XFEL in the photon energy region around 0.1 keV [7]. Thus, SACLA is now providing three XFELs in parallel and the experimental opportunity of SACLA is increased substantially.

Furthermore, SACLA has a beam transport line to the SPring-8 storage ring (XSBT) and the beam injection from SACLA to SPring-8 is planned in the near future. This is because the low-emittance upgrade of the SPring-8 storage ring was proposed [8] and the upgraded ring requires a low-emittance injection beam from SACLA. Therefore, a flexible beam route switching system is necessary to provide electron beams to both XFEL beamlines and the SPring-8 storage ring in parallel.

Since the XFEL photon energy is different for each experimental user, the electron beam energy for each beamline must be changed pulse-by-pulse. In addition, the optimum bunch length is different for each beamline [5], since the optics of each electron beam transport line is significantly different. Therefore, we are developing a flexible rf parameter switching system of each accelerator unit to change the beam parameter pulse-by-pulse.

In fact, we encountered an instability problem that the horizontal emittance and the horizontal pointing stability deteriorated after the dogleg beam transport line of BL2 [5]. Since this instability was suppressed for a longer bunch beam with a lower peak current, the cause of the instability was considered to be a coherent synchrotron radiation (CSR) effect. The rf parameter switching system helped the suppression of the CSR effect by stretching the bunch length for BL2. However, the XFEL intensity of BL2 was significantly smaller than BL3 in case of a longer bunch length. Therefore, an improvement of the optics of the BL2 dogleg part was necessary for the mitigation of the CSR effect to generate XFEL comparable to BL3.

In this article, we describe the design and operation status of the pulse-by-pulse beam route and parameter control system of SACLA. We also discuss the mitigation of the instability due to the CSR effect in the dogleg part of BL2.

<sup>†</sup>maesaka@spring8.or.jp

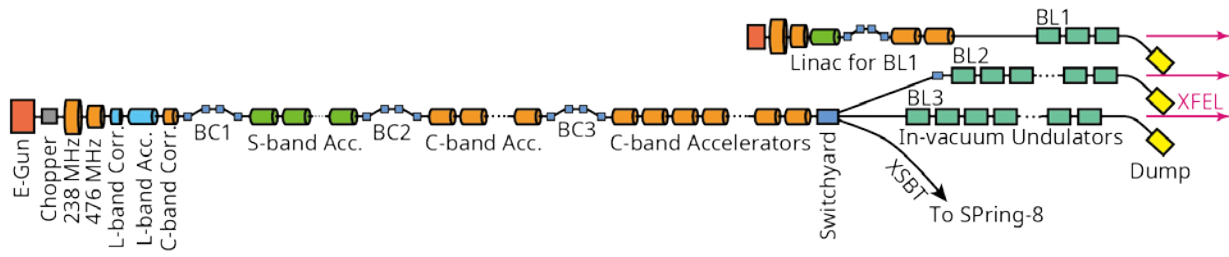


Figure 1: Schematic layout of SACLA.

## STRATEGY AND EQUIPMENTS FOR BEAM ROUTE AND PARAMETER CONTROL

The control items of the beam route and parameter control system are the beam route, the beam energy and the bunch length for each pulse. The beam route is switched by the kicker magnet in the switchyard. The beam energy is changed by turning on and off the triggers for accelerator units after the third bunch compressor, BC3. The bunch length is adjusted by changing the phases of accelerator units before BC3.

In this section, we introduce the development strategy of the pulse-by-pulse beam route and parameter control system. We then describe the beam switchyard for the beam route control including the transport line of BL2 and the timing and low-level rf (LLRF) system for each accelerator unit to change the beam energy and bunch length pulse-by-pulse.

### Development Strategy

The pulse-by-pulse beam parameter control system has been developed in two steps. The first step is to deliver electron beams to each beamline with an equal rate one after another. Since XFEL users prefer a constant interval between XFEL pulses, the condition of the first step is sufficient for the machine operation only for the XFEL beamlines. The second step is to switch the beam route and parameter in on-demand basis. Since the frequency of the beam injection to the SPring-8 storage ring during the top-up operation is 0.1 Hz or less, the beam route should be switched to XSBT only at an injection request. Therefore, on-demand switching of the beam route and parameter control is necessary for the beam injection from SACLA to SPring-8. We focus on the first step of the switching system in this section and we describe the second step in the later section.

### Beam Switchyard

The electron beam is distributed to each of BL2, BL3 and XSBT in the switchyard. The bending angles are  $+3^\circ$  for BL2,  $0^\circ$  for BL3 and  $-3^\circ$  for XSBT. The switchyard was initially equipped with a single DC bending magnet having the bending angle of  $\pm 3^\circ$ . We replaced the DC magnet with a combination of a kicker magnet and a twin-septum magnet in accordance with the construction of BL2 so as to switch the beam routes for individual 60 Hz bunches pulse-by-pulse [5]. The bending angle of the kicker and septum magnets are  $\pm 0.53^\circ$  and  $2.47^\circ$ , respectively. Magnet arrangements and beam optics

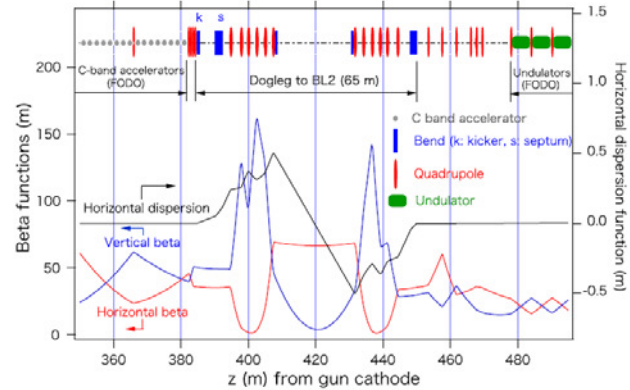


Figure 2: Magnet arrangements and beam optics around the BL2 dogleg in 2014. Dipole and quadrupole magnets are indicated by the blue and red symbols, respectively. Horizontal and vertical beta functions and a horizontal dispersion are plotted by red, blue and black lines, respectively.

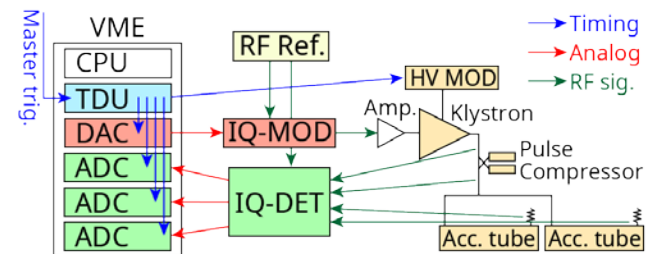


Figure 3: Schematic diagram of the timing and low-level rf system for each accelerator unit.

around the dogleg of BL2 is shown in Fig. 2. The optics of the dogleg was designed to be achromatic and it could also be made isochronous by using two small dipoles in the middle of the dogleg.

### Timing and Low-Level RF Control System

A schematic diagram of the timing and low-level rf system for each accelerator unit [9] is shown in Fig. 3. The rf signal for each accelerator is synthesized by an in-phase and quadrature modulator (IQ-MOD). The IQ baseband waveform is generated by a 238 MSPS VME-DAC module. The rf signal from each high power rf component is detected by an IQ detector (IQ-DET). The IQ baseband waveforms are digitized by 238 MSPS VME-ADC modules.

Trigger signals for a klystron high-voltage pulse modulator (HV MOD), VMA-DAC, ADC, etc. are generated by VME trigger delay unit (TDU). The TDU receives a

Content from this work may be used under the terms of the CC BY 3.0 licence (© 2018). Any distribution of this work must maintain attribution to the author(s), title of the work, publisher, and DOI.

60 Hz master trigger signal and outputs the trigger signal for each component at an appropriate timing.

### Beam Energy Control

The beam energy is changed pulse-by-pulse by turning on or off the trigger signals for some of the accelerator units [10]. The example of the energy control scheme is illustrated in Fig. 4. Since the VME-TDU has a frequency division function of the master trigger input, the trigger rate of each accelerator unit can be set individually. In case of Fig. 4, high and low energy beams are generated one after another with a total repetition rate of 60 Hz (30 Hz each). Since the acceleration voltage of each C-band unit is approximately 120 MeV, the beam energy can be changed in this energy step. Of course, the energy can be adjusted by changing the output rf power of the klystron. Although the quadrupole strength in the accelerator is the same for both high and low energy beams, the beam envelop can be matched by quadrupoles after the switchyard. We confirmed that two beams with the energy ratio of 1:2 could be appropriately accelerated and transported by the same quadrupole setting [10].

### Bunch Length Control

The bunch length is shortened by three bunch compressors in SACLA. Since the bunch compression ratio depends on the energy chirp generated by upstream accelerator units, the bunch length can be varied by adjusting the phase of the accelerator units. In contrast to the TDU utilized for beam energy control, the VME-DAC and ADC do not have the function to change behavior one after another. Therefore, we developed software to change the rf phase pulse-by-pulse, as shown in Fig. 5.

The MADOCA control system [11] used in SACLA controls the VME modules by the equipment manager (EM) on the VME-CPU. MADOCA can run some EM agent (EMA) processes for real-time control. The pulse-by-pulse rf parameter control is implemented to the EMA processes, EMA-SW, EMA-PID1 and EMA-PID2. EMA-SW accesses the IQ data to the DAC and from the ADC. EMA-PID1 and -PID2 regulate the phase of each beam route by proportional-integrate-differential (PID) control. The ADC data taken by EMA-SW is sorted to each of EMA-PID1 and -PID2 according to the trigger number from the TDU. The set values calculated by EMA-PID1 and -PID2 are sent to EMA-SW and written to DAC.

## DEMONSTRATION OF BUNCH LENGTH CONTROL

We tested the bunch length control software with an actual beam. The phase of one the C-band accelerator units in the upstream of BC3 was changed between bunching ( $-50^\circ$  from the crest) and debunching phases ( $+50^\circ$  from the crest) pulse-by-pulse. The bunch length was measured by a transverse rf deflector system after BC3 [12]. As shown in Fig. 6, the bunch length was compressed to 20 fs FWHM for the bunching phase and the 100 fs FWHM for the debunching phase. Thus, the bunch length was appropriately controlled pulse-by-pulse.

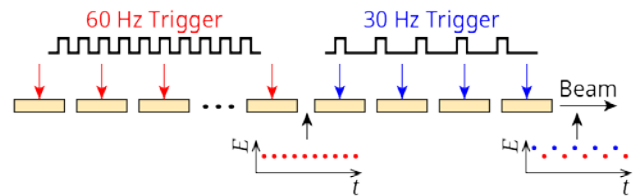


Figure 4: Pulse-by-pulse beam energy control scheme.

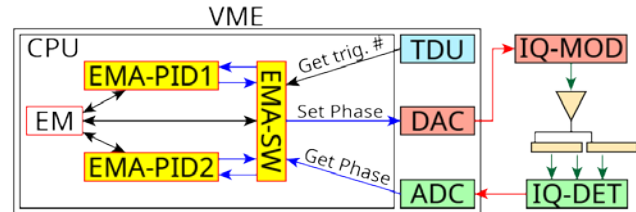


Figure 5: Schematic diagram of the rf parameter switching system.

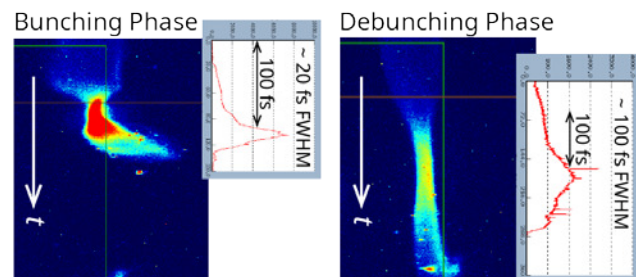


Figure 6: Bunch length measurement results with the rf deflector system. The left image shows a temporal profile for the bunching phase and the right one shows that for the debunching phase.

In this experiment, we found a large orbit distortion for the debunching phase, even though the orbit distortion was small enough for the bunching phase. The kick source of the orbit distortion was the accelerator used for the rf phase switching. Therefore, this orbit distortion was considered to be due to the phase-dependent focusing effect of the accelerator tube [13]. This kick indicates the displacement of the beam from the axis of the accelerator. Thus, the accelerator tubes should be precisely aligned, when the bunch length is largely changed pulse-by-pulse.

## MITIGATION OF THE CSR EFFECT IN THE BL2 DOGLEG PART

When the electron beam optimized for BL3 was transported to BL2, the XFEL intensity of BL2 did not exceed  $30 \mu\text{J}$  per pulse, corresponding to less than 1/10 of BL3 [5], due to the emittance growth and the pointing jitter degradation coming from the CSR effect. Even if we stretched the bunch length to reduce the CSR, the maximum XFEL intensity was still  $150 \mu\text{J}$  per pulse at most.

We found that the phase space distortion due to CSR at the upstream bend of the dogleg can be canceled out by the downstream one and the emittance growth can be diminished [14]. The new beam optics of the BL2 dogleg is shown in Fig. 7. The cancellation condition can be satisfied by using the double-bend achromat (DBA) lattice for both bends of the dogleg and by setting the beta-

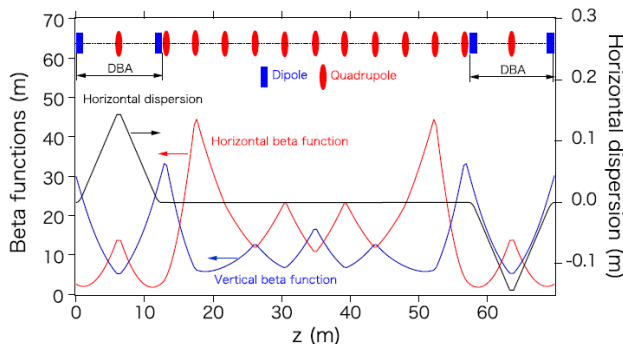


Figure 7: Magnet arrangement and beam optics of the new BL2 dogleg. The legend is the same as Fig. 2.

tron phase advance between the two DBAs to  $\pi$ . The quality of the electron beam, such as a 0.8 mm mrad emittance, a 10 kA peak current and a 10 fs FWHM bunch length, was almost conserved in the new dogleg, although the emittance deteriorated about one order of magnitude in the old dogleg case. We replaced the magnets of the BL2 dogleg in 2017 to mitigate the CSR effect. The deflection angle of the new kicker magnet is  $\pm 1.5^\circ$ , which is three times larger than the old one. Therefore, we developed a new kicker magnet power supply driven by SiC MOS-FETs [15].

To confirm the cancellation of the CSR effect after the replacement of the dogleg, we measured an electron beam pointing jitter with two rf cavity beam position monitors (BPM) [16]. The phase space distributions of the pointing jitter are plotted in Fig. 8. While the volumes of the vertical phase space distributions were almost same, the horizontal pointing jitter was significantly improved for the new optics.

Typical trend graphs of the XFEL intensities of BL2 and BL3 are plotted in Fig. 9. A beam energy, a photon energy and an undulator K-value were 7.8 GeV, 10 keV and 2.1, respectively, for both beamlines. The 60 Hz electron beam was equally distributed to the two beamlines (30 Hz each). The acceleration rf parameters for each beam-

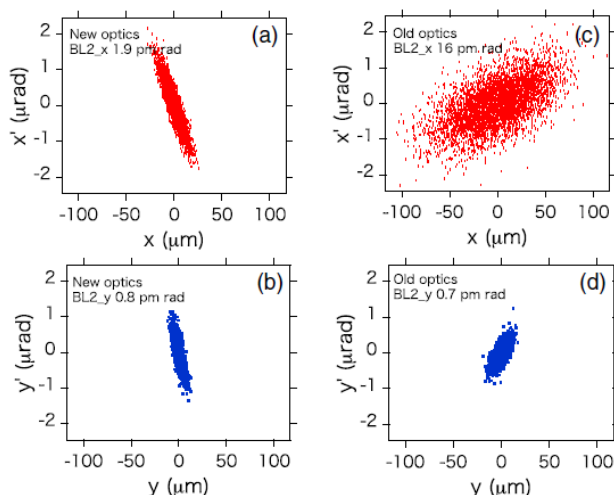


Figure 8: Horizontal (a, c) and vertical (b, d) phase space distributions of the electron beam pointing jitter after the BL2 dogleg for new (a, b) and old (c, d) optics.

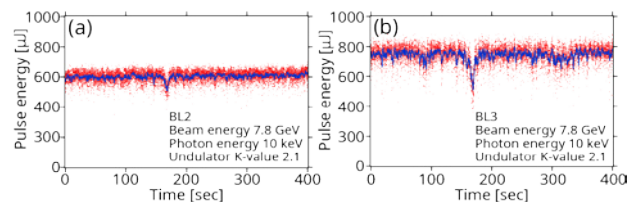


Figure 9: XFEL intensity trend graphs of BL2 and BL3 with pulse-by-pulse switching of the beam route and parameter.

line was individually optimized to maximize the XFEL intensity by using the rf parameter switching software described in the previous section. These graphs show that the XFEL intensities are comparable each other.

The rf phase for each beamline was slightly different, since the optimum bunch length depends on the optics of the transport line. The phase difference of the 238 MHz sub-harmonic buncher cavity, for example, was  $0.1^\circ$ . Thus, the rf parameter switching system has sufficient precision to adjust the bunch length of the electron beam for each beamline.

## DEVELOPMENT OF THE ON-DEMAND BEAM ROUTE AND PARAMETER SWITCHING SYSTEM

Toward the injection to the SPring-8 storage ring in parallel with the XFEL operation, we are developing an on-demand beam route and parameter switching system as the second step. A schematic diagram of this system is shown in Fig. 10. The beam route information is distributed pulse-by-pulse by using a reflective memory network. The interface to this network is realized by a mezzanine card mounted on the VME-CPU. The route information consists of the previous, current and next route numbers and the current master trigger number. The rf parameter for each accelerator unit, the current of the kicker magnet etc. are switched according to the route information. The route number, the rf parameters and the master trigger number are recorded by an event-synchronized data-acquisition (DAQ) system [17] pulse-by-pulse in order to check whether the beam parameter was switched appropriately or not.

The sequence of the on-demand switching system is summarized below:

1. DAQ takes the data related to the route and rf parameter switching (SW-DAQ) 16 ms after the previous master trigger.
2. DAQ starts taking the other data (All-DAQ) just after the end of SW-DAQ.
3. EMA-SW gets the route information just after the master trigger and sets the trigger and rf parameter 5 ms after the master trigger (SW-Set).

We tested the on-demand parameter switching system in a VME test bench in a laboratory and a linac for BL1. The beam route was switched by a given pattern of three or four beam routes. Some waveforms of the ADC modules were also acquired once a second to impose a certain load to the VME bus.

Content from this work may be used under the terms of the CC BY 3.0 licence (© 2018). Any distribution of this work must maintain attribution to the author(s), title of the work, publisher, and DOI.

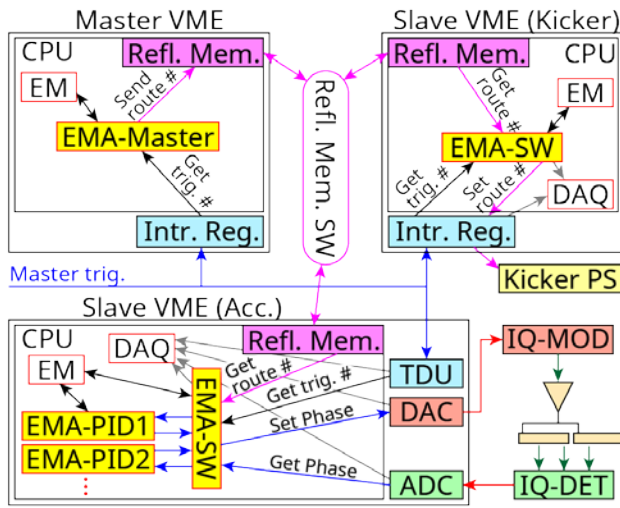


Figure 10: Schematic diagram of the on-demand beam route and parameter switching system.

The test setup in the test bench consists of two VMEs, one master VME and one slave VME. We executed an on-demand parameter switching software for more than 100 hours. The analysis of obtained data showed only one delay of parameter switching. This error rate is smaller than the other failures, such as a trip of the klystron high-voltage power supply.

For the evaluation in the linac for BL1, we used one master VME and four slave VMEs. The test data were taken for more than 40 hours and failure in the parameter switching was not found. Even though the only one inconsistency in the data was found, it was confirmed to be a delay of SW-DAQ and not to be the delay of EMA-SW itself. Figure 11 shows the histograms of the time stamp of SW-Set, SW-DAQ and All-DAQ. Although SW-DAQ must be done before the start of SW-Set, only one event (indicated by the red circle in the figure) was not in time with SW-Set. Since the parameter switching system is implemented by software, this kind of DAQ delay is unavoidable. However, the error rate is only  $1 \times 10^{-7}$  per pulse, which is smaller than the other failures. Thus, the parameter switching system can be used for the user operation of SACLA.

## SUMMARY

We installed a new XFEL beamline, BL2, in addition to BL3 and replaced the DC bending magnet with a kicker magnet in order to increase opportunities for user experiments by switching a beam route pulse-by-pulse. We also developed a beam route and rf parameter switching system to provide the optimized electron beam to each beamline. Although the XFEL performance of the initial version of the BL2 dogleg was not sufficient due to the CSR effect in the bending magnets, we modified the optics of the dogleg and the XFEL intensity comparable to BL3 was obtained in BL2. This result was achieved in combination with the rf parameter switching system, since the optimum beam parameters were slightly different even after the optics improvement. We are developing an on-demand beam route and parameter switching system

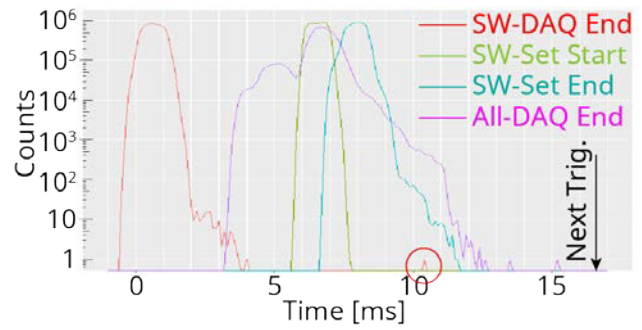


Figure 11: Histogram of the time stamp of the parameter switching and DAQ processes. Red, green, cyan and magenta lines show the end of DAQ for parameter switching, the start of parameter setting, the end of parameter setting and the end of all the DAQ. Horizontal axis is the delay time from the master trigger.

needed for beam injection to the SPring-8 storage ring. This system was tested in the test bench and the linac for BL1 and it worked well with sufficiently small failure rate of  $1 \times 10^{-7}$  per pulse. This new switching system will be in use in the next year.

## REFERENCES

- [1] T. Ishikawa *et al.*, “A compact X-ray free-electron laser emitting in the sub-ångström region”, *Nature Photonics*, vol. 6, pp. 540–544, 2012, doi:10.1038/NPHOTON.2012.141
- [2] K. Togawa *et al.*, “CeB<sub>6</sub> electron gun for low-emittance injector”, *Phys. Rev. ST Accel. Beams*, vol. 10, p. 020703, 2007, doi:10.1103/PhysRevSTAB.10.020703
- [3] T. Asaka *et al.*, “Low-emittance thermionic-gun-based injector for a compact free-electron laser”, *Phys. Rev. Accel. Beams*, vol. 20, p. 080702, 2017, doi:10.1103/PhysRevAccelBeams.20.080702
- [4] T. Inagaki *et al.*, “High-gradient C-band linac for a compact x-ray free-electron laser facility”, *Phys. Rev. ST Accel. Beams*, vol. 17, p. 080702, 2014, doi:10.1103/PhysRevSTAB.17.080702
- [5] T. Hara *et al.*, “Pulse-by-pulse multi-beamline operation for x-ray free-electron lasers”, *Phys. Rev. Accel. Beams*, vol. 19, p. 020703, 2016, doi:10.1103/PhysRevAccelBeams.19.020703
- [6] T. Shintake *et al.*, “A compact free-electron laser for generating coherent radiation in the extreme ultraviolet region”, *Nature Photonics*, vol. 2, pp. 555–559, 2008, doi:10.1038/NPHOTON.2008.134
- [7] K. Togawa *et al.*, “A Soft X-ray Free-Electron Laser Beamline of SACLA”, in *Proc. 8th Int. Particle Accelerator Conf. (IPAC'17)*, Copenhagen, Denmark, May 2017, pp. 1209–1212, doi:10.18429/JACoW-IPAC2017-TU0AA2
- [8] SPring-8-II Conceptual Design Report, Nov. 2014, <http://rsc.riken.jp/pdf/SPring-8-II.pdf>
- [9] Y. Otake *et al.*, “Timing and low-level rf system for an x-ray laser”, *Phys. Rev. Accel. Beams*, vol. 19, p. 022001, 2016, doi:10.1103/PhysRevAccelBeams.19.022001
- [10] T. Hara *et al.*, “Time-interleaved multienergy acceleration for an x-ray free-electron laser facility”, *Phys. Rev. ST Accel. Beams*, vol. 16, p. 080701, 2013, doi:10.1103/PhysRevSTAB.16.080701

- [11] T. Fukui *et al.*, “Status of the Control System for the SAC-LA/SPring-8 Accelerator Complex”, in *Proc. 16th Int. Conf. on Accelerator and Large Experimental Control System (ICALEPCS'17)*, Barcelona, Spain, Oct. 2017, pp. 1995–1999, doi:10.18429/JACoW-ICALEPCS2017-FRAPL03
- [12] Y. Otake *et al.*, “Beam monitor system for an x-ray free electron laser and compact laser”, *Phys. Rev. ST Accel. Beams*, vol. 16, p. 042802, 2013, doi:10.1103/PhysRevSTAB.16.042802
- [13] H. Maesaka *et al.*, “Analysis and Measurement of Focusing Effects in a Traveling Wave Linear Accelerator”, in *Proc. 35th Int. Free-Electron Laser Conf. (FEL'13)*, New York, USA, Aug. 2013, paper TUPSO46, pp. 329–333.
- [14] T. Hara *et al.*, “High peak current operation of x-ray free-electron laser multiple beam lines by suppressing coherent synchrotron radiation effects”, *Phys. Rev. Accel. Beams*, vol. 21, p. 040701, 2018, doi:10.1103/PhysRevAccelBeams.21.040701
- [15] C. Kondo *et al.*, “A stable pulsed power supply for multi-beamline XFEL operations”, *Rev. Sci. Instrum.*, vol. 89, p. 064704, 2018, doi:10.1063/1.5025109
- [16] H. Maesaka *et al.*, “Sub-micron resolution rf cavity beam position monitor system at the SACLA XFEL facility”, *Nucl. Instr. Meth., sec. A*, vol. 696, pp. 66–74, 2012, doi:10.1016/j.nima.2012.08.088
- [17] M. Yamaga *et al.*, “Event-Synchronized Data-Acquisition System for SPring-8 XFEL”, In *Proc. 12th Int. Conf. on Accelerator and Large Experimental Control System (ICALEPCS'09)*, Kobe, Japan, Oct. 2009, paper TUB003, pp.69–71.